DEVELOPMENT OF TERNARY DIAGRAMS FOR ESTIMATING WATER RETENTION PROPERTIES USING A GEOSTATISTICAL APPROACH

T. B. Ramos[1,*], M. C. Gonçalves[2], A. M. Horta[3], J. C. Martins[2], and L. S. Pereira[1]

[1] *CEER, Institute of Agronomy, University of Lisbon, Tapada da Ajuda, 1349-017 Lisbon, Portugal.*

[2] *INIAV, National Institute of Agronomic and Veterinarian Research, Av. República, 2784-505 Oeiras, Portugal.*

[3] *Department of Environmental Sciences, Faculty of Agriculture and Environment, The University of Sidney, Eveleigh NSW 2015, Australia.*

Abstract

Most pedotransfer functions (PTFs) have adopted soil texture information as the main predictor to estimate soil hydraulic properties, whether inputs are defined in terms of the relative proportion of different grain size particles or texture-based classifications. The objective of this study was to develop ternary diagrams for estimating soil water retention at -33 and -1500 kPa matric potentials, corresponding to the field capacity and wilting point, respectively, from particle size distribution using a geostatistical approach. The texture triangle was divided into a 1% grid of soil texture composition resulting in 4332 different soil textures. Measured soil water retention values determined in 742 soil horizons/layers located in Portugal were then used to develop and validate the ternary diagrams. The development subset included two-thirds of the data, and the validation subset the remaining samples. The soil water content values were displayed in the ternary diagram according to the coordinates given by the particles size distribution determined in the same soil samples. The measured

[*] Corresponding author: Tel.: +351 214403500; fax: +351 214416011; Email address: tiago_ramos@netcabo.pt (T.B. Ramos).

volumetric water content values were then interpolated to the remaining areas of the ternary diagrams using ordinary kriging. Uncertainty analysis resulted in a root mean square error of 0.040 and 0.033 cm^3 cm^{-3} obtained when comparing the interpolated water contents at -33 and -1500 kPa matric potentials values, respectively, with the measured ones included in the validation dataset. The estimation variance was also considered to access the uncertainty of the estimations. The available water content of Portuguese soils was then derived from both ternary diagrams. The ternary diagrams may thus serve as simplified tools for estimating water retention properties from particle size distribution and eventually serve as an alternative to the traditional statistical regression and data mining techniques used to derive PTFs.

Keywords: Field capacity; Ordinary kriging; Soil Texture; Uncertainty; Wilting point.

1. Introduction

Modern hydrologic modeling studies require a quantitative and precise understanding of soil hydraulic properties. That information is essential for a wide range of applications, such as research on soil and water conservation, irrigation scheduling, solute transport, virus and bacterial migration, plant growth, and plant stress. However, classical methods for direct measurement of soil hydraulic properties (Dane and Topp, 2002) are known to be costly, time consuming, and impractical for large-scale applications in which many samples are required to quantify the spatial and temporal variability of those properties. Hence, pedotransfer functions (PTFs) have been developed as an alternative to classical methods to indirectly estimate soil hydraulic properties from basic soil physical and chemical properties (Bouma, 1989; Vereecken et al., 1989; McBratney et al., 2002; Pachepsky and Rawls, 2004), thus overcoming some of the limitations mentioned earlier, especially when the objective is to characterise soil hydraulic properties at large scales.

Most of the available PTFs use soil-texture-based information as the main predictor to estimate the hydraulic behaviour of soils. This popular option is justified by the fact that soil texture characteristics are among the most easily measured soil properties, and also by the assumption that soil texture is the dominant soil variable in determining hydraulic properties, while other soil variables, such as bulk density or organic matter content, have a secondary effect (Twarakavi et al., 2010). The simplest texture based PTFs were developed to provide estimates of average soil water retention properties or hydraulic parameters for different texture classes (e.g., Wösten et al., 1995; Schaap and Leij, 1998; Bruand et al., 2003; Al Majou et al., 2008; Ramos et al., 2013a). More complex functions have also been developed by relating the particle size limits of the soil constituents to soil hydraulics using multiple regression analysis or data mining tools (e.g., Gupta and Larson, 1979; Saxton et al., 1986; Schaap et al., 2001; Nemes et al., 2006; Haghverdi et al., 2012). Although the hierarchical approaches followed in many of those studies showed that the accuracy of PTFs improved considerably when other variables (usually bulk density), rather than soil texture information alone, were used also as predictors, texture based PTFs have been considered to also provide reasonably accurate estimates of soil hydraulic properties for many research and technical applications (Vereecken et al., 2010).

Soil texture is normally represented in a ternary diagram, function of sand, silt and clay percentages, where the limits of the texture classes vary according to the texture classification system used. However, the soil texture triangle has also had more applications than simply grouping texture information data, namely it has also been used as a tool to estimate soil hydraulic properties. Saxton et al. (1986) divided the soil texture triangle into grids of 10% sand and 10% clay content increments to develop texture based PTFs for generalized predictions of soil hydraulic properties in each grid cell. Later, Saxton and Rawls (2006) updated the previous work to further include the effect of organic matter, bulk density, gravel, and salinity in their model and provide a broadly applicable predictive system. The developed model has been successfully applied to a wide variety of analysis, particularly those related to agricultural hydrology and water management, since estimates do not involve complex mathematical methods, and the texture triangle serves as a familiar tool to users for estimating the soil water characteristics. Twarakavi et al. (2010) also focused on the relations between the texture triangle and soil hydraulic properties. Those authors estimated soil hydraulic properties throughout the entire soil texture triangle as a function of sand, silt, and clay contents using the ROSETTA PTFs (Schaap et al., 2001) such that the various soil texture possibilities (i.e., combinations of sand, silt, and clay percentages) were considered. They then concluded that although the soil texture triangle was qualitatively very similar to the soil hydraulic triangle, differences existed especially for soils where capillary forces dominate the flow throughout the soils. Bormann (2007) took those studies one step forward and performed water balance calculations for the entire space of the soil texture triangle, after dividing it into 1% grid cells and applying Rawls and Brakensiek (1985) PTFs for obtaining the soil hydraulic properties.

In this study, a geostatistical approach was used to spatial interpolate water retention values (the field capacity and wilting point) available in a soil database (Gonçalves et al., 2011) throughout the entire soil texture triangle. Kriging is generally considered to be the best method for spatial interpolation that also includes information on uncertainty (Goovaerts, 1999, 2001). Although there are countless applications to its application in soil science, as far as we know the kriging estimator has never been used as a PTF to actually derive soil hydraulic properties from basic soil data. To proceed with this study, three very basic assumptions had to be validated:

(i) Soil texture and soil water retention properties available in the database were assumed as being determined in the same sample. This is usually not the case in most PTFs where the predictors used in their development, although measured in the same soil horizon, are not always determined directly on the soil samples used for measuring the hydraulic properties. As referred by Vereecken et al. (2010), this becomes more important as the spatial and temporal variability of additional soils information increase and the information content is not related anymore to the samples on which the hydraulic properties were determined. Thus, taking into account the size of the database used in this study, the error resulting from this assumption was not considered to be relevant.

(ii) Soil texture was assumed as the main predictor to estimate soil hydraulic properties. As mentioned earlier, this is the main assumption sustaining all texture based PTFs, since these two soil properties normally exhibit a high correlation.

(iii) The spatial continuity of soil hydraulic properties along the soil texture triangle could be described by means of a variogram. Taking into account that soil texture is the main soil property considered when grouping soils having similar water retention curves (Wösten et al., 1995; Bruand et al., 2003; Ramos et al., 2013a), and that the soil texture triangle and the soil hydraulic triangle can be relatively similar (Twarakavi et al., 2010), we assumed that there could be a spatial dependence of soil hydraulic properties, at least within the limits of each soil texture class. The percentage units that define the texture triangle were thus converted into metric units to allow the application of geostatistics.

The objective of this study is thus to develop ternary diagrams for estimating point specific water retention values (the field capacity and wilting point) of Portuguese soils using a geostatistical approach. The available water capacity was later computed from both ternary diagrams.

2. Material and Methods

2.1. The data set

The ternary diagrams were developed for estimating the field capacity and wilting point of Portuguese soils from particle size distribution. The field capacity and wilting point were here assumed to correspond to the water retention values at -33 and -1500 kPa, respectively. The data was extracted from the PROPSOLO soil database (Gonçalves et al., 2011), which gathers all information on soil hydraulic and pedological properties from soil profiles obtained from research projects and academic studies performed at the Portuguese National Institute of Agronomic and Veterinarian Research (former Estação Agronómica Nacional). This database contains practically all of the existing knowledge on the soil hydraulic properties of Portuguese soils (with the exception of a few specific retention points found in soil survey studies).

The data included information on soil texture and water retention properties of 742 horizons/layers studied in 346 soil profiles located in Portugal between 1977 and 2012 (Fig. 1). The soil reference groups (FAO, 2006) represented were Fluvisols (36.4%), Luvisols (29.5%), Vertisols (9.8%), Cambisols (8.7%), Calcisols (6.6%), Anthrosols (4.0%), Arenosols (1.4%), Podzols (0.9%), Regosols (0.9%), Ferralsols (0.6%), Leptosols (0.6%), and Planosols (0.6%).

The data was randomly divided in two subsets, a development set composed of two-thirds of the data (495 horizons/layers), and a validation set with the remaining one-third of the data (247 horizons/layers). Table 1 presents the main physical and chemical properties of the two datasets. The particle size distribution was obtained using the pipette method for particles having diameters <2 μm (clay) and between 20–2 μm (silt), and by sieving for particles between 200–20 μm (fine sand) and between 200–2000 μm (coarse sand). These textural classes follow the Portuguese classification system (Gomes and Silva, 1962) and are based on the International Soil Science Society (ISSS) particle limits (Atterberg scale). The organic carbon (OC) content was determined by the Walkley–Black method (Nelson and Sommers, 1982). The dry bulk density (ρ_b) was obtained by drying volumetric soil samples (100 cm^3) at 105 ºC for 48 h. The gravimetric water content at -33 kPa matric potential was determined on undisturbed soil samples (100 cm^3) using suction tables (Romano et al., 2002; used in 494 horizons/layers) or the pressure plate apparatus (Dane and Hopmans, 2002; used in 212 horizons/layers). The gravimetric water content at -1500 kPa matric potential was also determined on undisturbed soil samples (100 cm^3) using the pressure plate apparatus. Then, the volumetric water content for each horizon/layer and each matric potential was computed from the gravimetric water contents and the bulk density of the corresponding horizon/layer.

In the case of 36 soil horizons/layers where the volumetric water content at -33 kPa matric potential was not readily available, the missing values were estimated by introducing values derived from the fitted van Genuchten model (1980) to each individual water retention curve, also available in the soil database for all soil horizons/layers. The van Genuchten model describes the volumetric soil water content, θ (L^3 L^{-3}), as a function of matric potential, ψ (L), in the following form:

$$S_e(\psi) = \frac{\theta(\psi) - \theta_r}{\theta_s - \theta_r} = \frac{1}{\left(1 + |\alpha \psi|^{\eta}\right)^{1-1/\eta}} \tag{1}$$

in which S_e is the effective saturation, θ_r and θ_s denote the residual and saturated water contents (L^3 L^{-3}), respectively, α (L^{-1}) and η (-) are empirical shape parameters. This procedure introduced an error to the subsequent calculations and model evaluations resulting from the non-perfect fit of the fitted model to the experimental data (RMSE = 0.012 cm^3 cm^{-3}), in line with published results (e.g., Nemes and Rawls, 2006; Ramos et al., 2013a). The errors were thus relatively small compared with the errors usually obtained using PTFs, and therefore, the fitted values were assumed as if they were measured.

2.2. Development of the ternary diagrams

The soil texture triangle was divided into a 1% grid of soil texture composition resulting in 4332 different soil textures (i.e., different combinations of sand, silt, and clay percentages). Figure 2 shows the textural distribution of the datasets used for the development of the ternary diagrams and for their validation. The soil texture triangle was converted into ternary diagrams by replacing the percentage units by metric units (cm were used for convenience), and by including the soil water retention values at -33 and -1500 kPa matric potentials in the coordinates given by the particles size distribution determined in the same soil samples. Measured $\theta_{-33\ kPa}$ and $\theta_{-1500\ kPa}$ within the same location (i.e., same particle size distribution) were averaged. The measured volumetric water content values $\theta_{-33\ kPa}$ and $\theta_{-1500\ kPa}$ were then interpolated to the remaining areas of the ternary diagrams using ordinary kriging.

The spatial pattern of $\theta_{-33\ kPa}$ and $\theta_{-1500\ kPa}$ in each ternary diagram was first described from the semi-variance of the differences between measured values included in the development set using the experimental semivariogram (Goovaerts, 1997; Yates and Warrick, 2002), as follows:

$$\gamma_e(h) = \frac{1}{2\,n(h)} \sum_{i=1}^{n(h)} \left[Z(x_i) - Z(x_{i+h})\right]^2 \qquad (2)$$

where n(h) is the total number of pairs of observation points (x_i and x_{i+h}; i = 1, …, n) of the variable Z (i.e., $\theta_{-33\ kPa}$ and $\theta_{-1500\ kPa}$) that are separated by a distance h. The omnidirectional semivariogram was computed, and hence the spatial variability was assumed to be identical in all directions. The variogram was defined by assigning pairs of measured values of $\theta_{-33\ kPa}$ and $\theta_{-1500\ kPa}$ to a lag interval of 5 cm (h_i = i 5 cm), since data was irregularly distributed in the texture triangle (Fig. 2). A theoretical variogram was then fitted to the experimental semivariogram using a Gaussian model with nugget effect (Goovaerts, 1997; Yates and Warrick, 2002):

$$\gamma_t(h) = \begin{cases} C_0 + C_1 \left[1 - \exp\left(\dfrac{-3\,h^2}{a^2} \right) \right] & \text{for } h \le a \\ C_0 + C_1 & \text{for } h > a \end{cases} \tag{3}$$

where C_0 is the nugget (-), C_1 is the sill (-), and a is the range (L). The nugget, C_0, is a measure of discontinuity at the origin of the semivariogram which mainly arises from various sources of unexplained errors, such as measurement errors or the existence of spatial variations at distances smaller than the shortest sampling interval. The sill, C_1, should be approximately equal to the variance of the data. Finally, the range, a, corresponds to the distance at which the semivariance approaches the sill, and represents the separation distance beyond which two values of the variable can be considered statistically independent.

Ordinary kriging was the geostatistical interpolation method selected (Goovaerts, 1997; Yates and Warrick, 2002). The kriging estimator, $Z^*(x)$, provided an estimate of $\theta_{-33\ kPa}$ and $\theta_{-1500\ kPa}$ at a location x_0 of the ternary diagram that contained no information. The estimator is written as a linear combination of the measured values, $Z(x_i)$, that is,

$$Z^*(x_0) = \sum_{i=1}^{n} \lambda_i Z(x_i) \tag{4}$$

where the observation at each location was weighted by λ_i. The value of λ_i depended on its proximity and orientation to x_0 and to the other sample locations, x_i. Since by definition,

$$E\left[Z^*(x_0)\right] = \sum_{i=1}^{n} \lambda_i \; E\left[Z(x_i)\right] \tag{5}$$

and

$$E\left[Z(x)\right] = m \tag{6}$$

the estimates will be unbiased (i.e., $E[Z(x) - Z^*(x_0)] = 0$). The following ordinary kriging system was solved in order to minimize the prediction variance:

$$\begin{cases} \sum_{i=1}^{n} \lambda_i \, \gamma(x_k - x_i) + \mu = \gamma(x_k - x_0) \\ \sum_{i=1}^{n} \lambda_i = 1 \end{cases} \tag{7}$$

where E[ ] is the expected value, m is the mean value of Z(x), γ is the semivariance between data pairs, μ is the Lagrange parameter accounting for the constraint on the weights, and k = 1, …, n.

The variograms calculation and fitting, and the implementation of the kriging method were carried out with the geoMS software package (CMRP, 2000).

2.3. Uncertainty analyses

The uncertainty of the ordinary kriging interpolation estimates was considered to be the estimation variance in each grid cell of the ternary diagrams. The estimation variance σ^2 gives an indication of the quality of the estimates and was computed as follows (Goovaerts, 1997; Yates and Warrick, 2002),

$$\sigma_k^2(x_0) = \sum_{i=1}^{n} \lambda_i \, \gamma(x_i - x_0) + \mu \tag{8}$$

The ternary diagrams were also validated by comparing measured $\theta_{-33\ kPa}$ and $\theta_{-1500\ kPa}$ values included in the validation dataset with ordinary kriging estimates using various quantitative measures of the uncertainty, such as the determination coefficient (R^2), the mean error (ME), and the root mean square error (RMSE), given by:

$$R^2 = \left[\frac{\sum_{i=1}^{n} \left(O_i - \bar{O}\right)\left(P_i - \bar{P}\right)}{\left[\sum_{i=1}^{n} \left(O_i - \bar{O}\right)^2\right]^{0.5} \left[\sum_{i=1}^{n} \left(P_i - \bar{P}\right)^2\right]^{0.5}} \right]^2 \tag{9}$$

$$ME = \frac{1}{n} \sum_{i=1}^{n} (P_i - O_i) \tag{10}$$

$$\mathrm{RMSE} = \sqrt{\frac{\sum_{i=1}^{n}\left(P_i - O_i\right)^2}{n-1}} \qquad (11)$$

where n is the number of observations, O_i are the measured values, P_i are the interpolation predictions, $\overline{O}$ is the average of the measured values, and $\overline{P}$ is the average of the interpolation predictions.

3. Results and Discussion

3.1. Spatial patterns of $\theta_{-33\ kPa}$ and $\theta_{-1500\ kPa}$

Figure 3 presents the experimental and theoretical semivariograms obtained for $\theta_{-33\ kPa}$ and $\theta_{-1500\ kPa}$. The fitted parameters of the Gaussian model are given in Table 2. The nugget value found for $\theta_{-33\ kPa}$ and $\theta_{-1500\ kPa}$ corresponded to 15.4 and 6.1% of the total variance (C), respectively. As referred above, these values can be explained by sampling or measurement errors, and by variability that occurs at scales too small to characterize, which in this case correspond to variability that cannot be explained only by variations in soil texture. This unexplained variability is surely attributed to the effect of bulk density, organic matter, soil structure, soil mineralogy, soil chemical composition, and land use and management on water retention properties. Like in the development of traditional PTFs, grouping data by considering the effect of those soil properties (Wösten et al., 2001) would likely be advantageous in order to reduce the unexplained variability found in the development of the ternary diagrams. However, that approach would require a much larger database than the one currently available. The larger nugget value found for the semivariogram of $\theta_{-33\ kPa}$ may be further related to the different methodologies used for measuring water retention at -33 kPa matric potential (Schaap and Leij, 1998).

The spatial continuity of $\theta_{-33\ kPa}$ and $\theta_{-1500\ kPa}$ reached a range of 39.7 and 24.6 cm in the ternary diagrams, respectively. Water retention values were thus correlated with samples located in neighbor texture classes, but more distanced areas of the texture triangle showed no correlation with those measured values. These findings seem to be very useful to understand the limitations of the simplest texture based PTFs, the class-PTFs (Wösten et al., 2001), when estimating water retention properties for different texture classes. These class-PTFs estimate average soil water retention properties for different texture classes based on the arithmetic (e.g., Bruand et al., 2003; Al Majou et al., 2008; Ramos et al., 2013a) or geometric mean (e.g., Wösten et al., 1995, 1999) of the datasets. However, for most regions of the texture triangle water retention values are sometimes better correlated with data included in their vicinity which may well be included in a neighbor texture class.

3.2. Ternary diagrams

Figure 4 presents the ternary diagram developed by ordinary kriging for estimating $\theta_{-33\ kPa}$ from particle size distribution. The resulting estimation variance is also shown in the same figure. Soil water retention values at -33 kPa matric potential were lower in the coarser texture classes and increased gradually with the increment of clay and silt contents. Basically, the ordinary kriging method calculated $\theta_{-33\ kPa}$ for all 4332 grid cells of the ternary diagram as a kind of weighted average of the measured values in the vicinity of each grid cell. The neighboring sample point values were weighted according to the semivariance as a function of distance to the prediction location. The kriging method also compensated for the effects of data clustering, by assigning individual points within a cluster less weight than isolated data points. This showed to be particularly useful when interpolating water content values to regions of the texture triangle where the information available in the development set was scarcer.

The mean and standard deviation values of the interpolated $\theta_{-33\ kPa}$ ternary diagram were 0.365 and 0.086 $cm^3\ cm^{-3}$, respectively. The mean value was thus higher than the one registered in the development dataset (0.287 $cm^3\ cm^{-3}$; Table 1). The difference found resulted from the fact that the interpolated ternary diagram estimated $\theta_{-33\ kPa}$ for all 4332 soil textures, including regions of the texture triangle where the development dataset had no information (e.g., the silty texture class, and the region of the texture triangle with clay content higher than 65%), thus producing significant differences in the classes of the interpolated histogram with higher water contents (not shown). The estimation variance was very high in those regions, and thus local estimates of $\theta_{-33\ kPa}$ were not realistic (Fig. 4). For the remaining regions of the ternary diagram, the estimation variance was low and estimates were considered to be accurate. In these regions, the mean value given by the kriging estimator ($m = 0.338\ cm^3\ cm^{-3}$ where, for example, $\sigma^2 \leq 0.002$) and the mean value of the development dataset tended to be closer.

Figure 5 presents the interpolated $\theta_{-1500\ kPa}$ ternary diagram and the respective estimation variance. Soil water retention values at -1500 kPa matric potential were also lower in the coarser texture classes and increased progressively with the increase of clay content. However, soil water retention did not increase as gradually as registered for the $\theta_{-33\ kPa}$ ternary diagram, since there are a few regions of the texture triangle (e.g., the area in the vicinity of the soil texture with 50% clay, 32% silt, and 18% sand) that clearly needed more information when estimating $\theta_{-1500\ kPa}$. The mean and standard deviation values of the interpolated $\theta_{-1500\ kPa}$ ternary diagram were 0.216 and 0.101 $cm^3\ cm^{-3}$, respectively. The mean value was once again higher than the one in the development dataset (0.162 $cm^3\ cm^{-3}$; Table 1), but it was slightly lower where $\sigma^2 \leq 0.002$ ($m = 0.204\ cm^3\ cm^{-3}$).

The results of the goodness-of-fit tests between measured and estimated water retention values at both matric potentials are presented in Table 3. Figure 6 shows the corresponding scatter plots between measured and estimated values. The kriging method produced an acceptable estimation of $\theta_{-33\ kPa}$ and $\theta_{-1500\ kPa}$, with ME values being very close to zero. RMSE values also showed that estimates were relatively accurate. RMSE were 0.040 and 0.033 $cm^3\ cm^{-3}$ for the estimates of $\theta_{-33\ kPa}$ and $\theta_{-1500\ kPa}$, respectively. The R^2 values were considerably high and identical for both water contents ($R^2 > 0.78$), indicating also a good agreement between measurements and predictions. However, data in the $\theta_{-1500\ kPa}$ scatter plot was found to be slightly more dispersing than for $\theta_{-33\ kPa}$.

Table 4 shows the accuracy of published PTFs that are available for estimating soil hydraulic properties of Portuguese soils, and which estimates can be compared with those obtained with the ternary diagrams. We limited our comparison to PTFs that used partially or the entire dataset used in this study. The class-PTFs developed by Ramos et al. (2013a) produced RMSE values that varied between 0.042 and 0.055 $cm^3\ cm^{-3}$ when estimating $\theta_{-33\ kPa}$, and between 0.037 and 0.048 $cm^3\ cm^{-3}$ when predicting $\theta_{-1500\ kPa}$. The best estimates, achieved with the class-PTFs developed after grouping data by ISSS texture classes and bulk density, can be comparable with the estimates given by the ternary diagrams. The point PTFs developed by Ramos et al. (2013b) yielded RMSE values of 0.040 and 0.036 $cm^3\ cm^{-3}$ also when predicting $\theta_{-33\ kPa}$ and $\theta_{-1500\ kPa}$, respectively, thus producing very similar predictions to those given by the kriging method. On the other hand, the parametric PTFs developed by Gonçalves et al. (1997), Wösten et al. (1999), and Ramos et al. (2013b) resulted in slightly higher RMSE values ($\geq 0.046\ cm^3\ cm^{-3}$) than those calculated with estimates given by the ternary diagrams. Hence, Table 4 shows that similar or even better predictions of $\theta_{-33\ kPa}$ and $\theta_{-1500\ kPa}$ can be obtained with the ternary diagrams. The only predictor needed is the particle size distribution, while the other comparable PTFs require relatively more predictors than the needs of those diagrams. In terms of number of predictors, the ternary diagrams seem to be quite useful as they are the only PTFs that do not require bulk density, despite results are given in terms of volumetric water contents. Although this soil property is simple to measure, sampling undisturbed samples in different soil horizons/layers distributed over large areas in order to measure bulk density may be a very laborious task.

3.3. Available water capacity

Figure 7 shows estimates of the available water capacity (AWC), calculated as the difference between $\theta_{-33\ kPa}$ and $\theta_{-1500\ kPa}$, and setting soil depth to 1 m as reference for comparison between estimates. AWC was only calculated for areas of the ternary diagrams where the estimation variance of either $\theta_{-33\ kPa}$ or $\theta_{-1500\ kPa}$ was lower than 0.002. This value was chosen arbitrarily, but is much lower than the dataset total variance (Table 2). Therefore, we only considered estimates than may be considered reliable and avoided extrapolations produced by the kriging estimator.

The largest AWC estimates were obtained for the medium fine texture classes. The coarser texture classes and the soils with 65% clay content seem to present lower AWC. However, the low estimates found for these latter soils are produced in a region of the ternary diagram where the estimation variance increases rapidly with the increase of the clay content, i.e., those predictions are near the limits of a region where the kriging estimator starts to extrapolate information instead of interpolating it, and thus care should be taken when using that information. Nevertheless, the histogram presented in Fig. 8 shows that estimates of the AWC have an average value of 134.1 mm/m, a variance of 3150.7, and kurtosis (0.45) and skewness (0.83) close to zero. However, the Chi-Square and Kolmogorov-Smirnov (p value = 0.00 < 0.01) goodness-of-fit tests rejected the hypothesis that AWC is normally distributed at a level of 99% confidence since soil water content information in the very fine and medium fine texture classes is missing.

The ternary diagrams developed in this study ($\theta_{-33\ kPa}$, $\theta_{-1500\ kPa}$, and AWC) may potentially be useful for many scientific and technical domains, but they seem more relevant to agricultural water management, particularly irrigation management and scheduling. Various water balance models require the type of information provided by the ternary diagrams here developed at point scale (Liu et al., 1998; George et al., 2000; Chopart et al., 2007; Steduto et al., 2009; Khaledian et al., 2009; Rosa et al., 2012). Those that are associated to a geographical information system and are applied at field scale (Troch et al, 1993; Fortes et al., 2005; Ojeda-Bustamante et al., 2007) can make even further use of the ternary diagrams here developed for estimating soil water retention properties of Portuguese soils.

4. Conclusions

The geostatistical approach was able to provide reliable estimates of soil water retention at -33 and -1500 kPa matric potentials using only the relative proportion of different grain size particles (sand, silt, and clay) as input data. The ordinary kriging method was helpful to understand which estimates of the soil water retention were valid based on the values of the estimation variance, and thus extrapolations were avoided.

The RMSE values were 0.040 and 0.033 $cm^3\ cm^{-3}$ when comparing the estimates provided by the $\theta_{-33\ kPa}$ and $\theta_{-1500\ kPa}$ ternary diagrams, respectively, and the measured values included in the validation dataset. Those values are comparable to the estimates provided by most of the available PTFs for estimating soil water retention properties of Portuguese soils. The ternary diagrams may thus serve as simplified tools for estimating those properties from particle size distribution and eventually serve as an alternative to the traditional statistical regression and data mining techniques used to derive PTFs.

Acknowledgments

This research was performed within the framework of the Project PTDC/AGR-AAM/098100/2008 of the Fundação para a Ciência e a Tecnologia (FCT). T. B. Ramos was funded by the FCT grant SFRH/BD/60363/2009.

References

Al Majou, H., Bruand, A., Duval, O., Le Bas, C., Vautier, A., 2008. Prediction of soil water retention properties after stratification by combining texture, bulk density and the type of horizon. Soil Use and Management 24, 383-391, doi:10.1111/j.1475-2743.2008.00180.x.

Bormann, H., 2007. Analysis of the suitability of the German soil texture classification for the regional scale application of physical based hydrological model. Advances in Geoscience 11, 7-13, doi:10.5194/adgeo-11-7-2007.

Bouma, J., 1989. Using soil survey data for quantitative land evaluation. Advances in Soil Science 9, 177-213.

Bruand, A., Pérez Fernandez, P., Duval, O., 2003. Use of class pedotransfer functions based on texture and bulk density of clods to generate water retention curves. Soil Use and Management 19, 232-242, doi:10.1111/j.1475-2743.2003.tb00309.x.

Chopart, J.L., Mézino, M., Aure, F., Le Mézo, L., Mété, M., Vauclin, M., 2007. OSIRI: A simple decision-making tool for monitoring irrigation of small farms in heterogeneous environments. Agricultural Water Management 87, 128-138, doi:10.1016/j.agwat.2006.06.023.

CMRP (Centro de Modelização de Reservatórios Petrolíferos), 2000. Manual do geoMS v1.0. Instituto Superior Técnico, Lisboa, Portugal.

Dane, J.H., Hopmans, J.W., 2002. Pressure plate extractor. In: Dane, J.H., Topp, G.C. (Eds.), Methods of Soil Analysis, Part 4, Physical Methods. Soil Science Society of America book Series, Madison, Wisconsin, pp. 688-690.

Dane, J.H., Topp, G.C., 2002. Methods of soil analysis. Part 4, Physical methods. Soil Science Society of America book Series, Madison, Wisconsin.

FAO, 2006. World reference base for soil resources. A framework for international classification, correlation and communication. World Soil Resources Report 103, Food and Agriculture Organization of the United Nations, Rome, Italy.

Fortes, P.S., Platonov, A.E., Pereira, L.S., 2005. GISAREG – A GIS based irrigation scheduling simulation model to support improved water use. Agricultural Water Management 77, 159-179, doi:10.1016/j.agwat.2004.09.042.

George, B.A., Shende, S.A., Raghuwanshi, N.S., 2000. Development and testing of an irrigation scheduling model. Agricultural Water Management 46, 121–136, doi:10.1016/S0378-3774(00)00083-4.

Gomes, M.P., Silva, A.A., 1962. Um novo diagrama triangular para a classificação básica da textura do solo. Garcia da Orta 10, 171–179.

Gonçalves, M.C., Pereira, L.S., Leij, F.J., 1997. Pedo-transfer functions for estimating unsaturated hydraulic properties of Portuguese soils. European Journal of Soil Science 48, 387-400, doi:10.1111/j.1365-2389.1997.tb00205.x.

Gonçalves, M.C., Ramos, T.B., Pires, F.P., 2011. Base de dados georreferenciada das propriedades do solo. In: Coelho, P.S., Reis, P. (Eds.), Agrorrural. Contributos Científicos. Instituto Nacional dos Recursos Biológicos, Oeiras, Portugal, pp. 564-574.

Goovaerts, P., 1997. Geostatistics for natural resources evaluation. Oxford University Press, New York.

Goovaerts, P., 1999. Geostatistics in soil science: state-of-the-art and perspectives. Geoderma 89, 1-45, doi:10.1016/S0016-7061(98)00078-0.

Goovaerts, P., 2001. Geostatistical modeling of uncertainty in soil science. Geoderma 103, 3-26, doi:10.1016/S0016-7061(01)00067-2.

Gupta, S.C., Larson, W.E., 1979. Estimating soil water retention characteristics from particle size distribution, organic matter content, and bulk density. Water Resources Research 15, 1633-1635, doi:10.1029/WR015i006p01633.

Haghverdi, A., Cornelis, W.M., Ghahraman, B., 2012. A pseudo-continuous neural network approach for developing water retention pedotransfer functions with limited data. Journal of Hydrology 442-443, 46-54, doi:10.1016/j.jhydrol.2012.03.036.

Khaledian, M.R., Mailhol, J.C., Ruelle, P., Rosique, P., 2009. Adapting PILOTE model for water and yield management under direct seeding system: The case of corn and durum wheat in a Mediterranean context. Agricultural Water Management 96, 757–770, doi:10.1016/j.agwat.2008.10.011.

Liu, Y., Teixeira, J.L., Zhang, H.J., Pereira, L.S., 1998. Model validation and crop coefficients for irrigation scheduling in the North China Plain. Agricultural Water Management 36: 233-246, doi:10.1016/S0378-3774(97)00051-6.

McBratney, A.B., Minasny, B., Cattle, S.R., Vervoort, R.W., 2002. From pedotransfer functions to soil inference systems. Geoderma 109, 41–73, doi:10.1016/S0016-7061(02)00139-8.

Nelson, D.W., Sommers, L.E., 1982. Total carbon, organic carbon, and organic matter. In: Page, A.L., et al. (Eds.), Methods of soil analysis, Part 2, Chemical and microbiological properties. ASA and SSSA, Madison, WI, pp. 539–579.

Nemes, A., Rawls, W.J., 2006. Evaluation of different representations of the particle-size distribution to predict soil water retention. Geoderma 132, 47-58, doi:10.1016/j.geoderma.2005.04.018.

Nemes, A., Rawls, W.J., Pachepsky, Y.A., 2006. Use of a nonparametric nearest-neighbor technique to estimate soil water retention. Soil Science Society of America Journal 70, 327–336, doi:10.2136/sssaj2005.0128.

Pachepsky, Y.A., Rawls, W.J., 2004. Development of pedotransfer functions in soil hydrology. Elsevier, Amsterdam, The Netherlands.

Ojeda-Bustamante, W., González-Camacho, J.M., Sifuentes-Ibarra, E., Isidro, E., Rendón-Pimentel, L., 2007. Using spatial information systems to improve water management in México. Agricultural Water Management 89, 81-88, doi:10.1016/j.agwat.2006.11.002.

Ramos, T.B., Gonçalves, M.C., Brito, D., Martins, J.C., Pereira, L.S., 2013a. Development of class pedotransfer functions for integrating water retention properties into Portuguese soil maps. Soil Research 51, doi:10.1071/SR12347.

Ramos, T.B., Gonçalves, M.C., Martins, J.C., Pereira, L.S., 2013b. Comparação de diferentes funções de pedotransferência para estimar as propriedades hidráulicas em Portugal. In: Gonçalves, M.C., Martins, J.C. (Eds.), Proceedings do Encontro Anual de Ciência do Solo, 26-28 Julho, Instituto Nacional de Investigação Agrária e Veterinária, Oeiras, Portugal.

Rawls, W.J., Brakensiek, D.L., 1985. Prediction of soil water properties for hydrologic modelling. In: Jones, E., Ward, T.J. (Eds.), Watershed management in the Eighties (Proceedings). ASCE, Denver, Colorado, pp. 293-299.

Romano, N., Hopmans, J.W., Dane, J.H., 2002. Suction table. In: Dane, J.H., Topp, G.C., (Eds.), Methods of Soil Analysis, Part 4, Physical Methods. Soil Science Society of America Book Series, Madison, Wisconsin, pp. 692-698.

Rosa, R., Paredes, P., Rodrigues, G.C., Alves, I., Fernando, R.M., Pereira, L.S., Allen, R.G., 2012. Implementing the dual crop coefficient approach in interactive software. 1. Background and computational strategy. Agricultural Water Management 103, 8-24, doi:10.1016/j.agwat.2011.10.013

Saxton, K.E., Rawls, W.J., Romberger, J.S., Papendick, R.I., 1986. Estimating generalized soil water characteristics from texture. Soil Science Society of America Journal 50, 1031–1036, doi:10.2136/sssaj1986.03615995005000040039x.

Saxton, K.E., Rawls, W.J., 2006. Soil water characteristics estimates by texture and organic matter for hydrologic solutions. Soil Science Society of America Journal 70, 1569–1578, doi:10.2136/sssaj2005.0117.

Schaap, M.G., Leij, F.J., 1998. Database-related accuracy and uncertainty of pedotransfer functions. Soil Science 163, 765-779, doi:10.1097/00010694-199810000-00001.

Schaap, M.G., Leij, F.J., van Genuchten, M.Th., 2001. ROSETTA: a computer program for estimating soil hydraulic parameters with hierarchical pedotransfer functions. Journal of Hydrology 251, 163-176, doi:10.1016/S0022-1694(01)00466-8.

Steduto, P., Hsiao, T.C., Raes, D., Fereres, E., 2009. AquaCrop — The FAO Crop Model to Simulate Yield Response to Water: I. Concepts and Underlying Principles. Agronomy Journal 101, 426-437, doi:10.2134/agronj2008.0139s.

Troch, P.A., Mancini, M., Paniconi, C., Wood, E.F., 1993. Evaluation of a distributed catchment scale water balance model. Water Resources Research 29, 1805–1817, doi:10.1029/93WR00398.

Twarakavi, N.K.C., Šimůnek, J, Schaap, M.G., 2010. Can texture-based classification optimally classify soils with respect to soil hydraulics? Water Resources Research 46, W01501, doi:10.1029/2009WR007939.

van Genuchten, M.Th., 1980. A closed form equation for predicting the hydraulic conductivity of unsaturated soils. Soil Science Society of America Journal 44, 892-898, doi:10.2136/sssaj1980.03615995004400050002x.

Vereecken, H., Maes, J., Feyen, J., Darius, P., 1989. Estimating the soil moisture retention characteristics from texture, bulk density, and carbon content. Soil Science 148, 389-403.

Vereecken, H., Weynants, M., Javaux, M., Pachepsky, Y., Schaap, M.G., van Genuchten, M.Th., 2010. Using pedotransfer functions to estimate the van Genuchten-Mualem soil hydraulic properties: a review. Vadose Zone Journal 9, 795-820, doi:10.2136/vzj2010.0045.

Wösten, J.H.M., Finke, P.A., Jansen, M.J.W., 1995. Comparison of class and continuous pedotransfer functions to generate soil hydraulic characteristics. Geoderma 66, 227-237, doi:10.1016/0016-7061(94)00079-P.

Wösten, J.H.M., Lilly, A., Nemes, A., Le Bas, C., 1999. Development and use of a database of hydraulic properties of European soils. Geoderma 90, 169-185, doi:10.1016/S0016-7061(98)00132-3.

Wösten, J.H.M., Pachepsky, Y.A., Rawls, W.J., 2001. Pedotransfer functions: bridging the gap between available basic soil data and missing soil hydraulic characteristics. Journal of Hydrology 251, 123-150, doi:10.1016/S0022-1694(01)00464-4.

Yates, S.R., Warrick, A.W., 2002. Geostatistics. In: Dane, J.H., Topp, G.C. (Eds.), Methods of Soil Analysis, Part 4, Physical Methods. Soil Science Society of America book Series, Madison, Wisconsin, pp. 81-118.

List of Tables

Table 1

Main physical and chemical properties of the datasets used in the development and validation of the ternary diagrams.

Statistics	Particle size distribution				Organic carbon	Bulk density	Volumetric water contents	
	2000-200 µm	200-20 µm	20-2 µm	<2 µm			$\theta_{-33\ kPa}$	$\theta_{-1500\ kPa}$
	(%)				(g kg^{-1})	(g cm^{-3})	(cm^3 cm^{-3})	
Development set (n = 495)								
Mean	20.7	34.5	21.6	23.2	0.74	1.50	0.287	0.162
Std. Deviation	17.7	15.2	11.8	14.7	0.54	0.18	0.089	0.081
Minimum	0.1	0.7	1.1	0.6	0.00	0.91	0.029	0.007
Maximum	94.4	70.7	68.1	63.3	2.51	1.90	0.536	0.407
Validation set (n = 247)								
Mean	21.4	34.7	20.5	23.4	0.72	1.52	0.282	0.158
Std. Deviation	17.1	15.4	12.4	14.3	0.52	0.18	0.086	0.073
Minimum	0.1	0.8	0.9	0.1	0.00	0.92	0.029	0.006
Maximum	94.6	73.6	60.2	62.2	2.21	1.87	0.535	0.359

Table 2

Parameters of the Gaussian model fitted to the experimental semivariograms.

Volumetric water contents	Nugget C_0 (-)	Sill C_1 (-)	Total variance C (-)	Range a (cm)
$\theta_{-33\ kPa}$	0.0012	0.0078	0.009	39.745
$\theta_{-1500\ kPa}$	0.0004	0.0066	0.007	24.604

Table 3

Results of the statistical analysis between measured water retention values at -33 and -1500 kPa and ordinary kriging estimates.

Statistics	Volumetric water contents	
	$\theta_{-33\ kPa}$	$\theta_{-1500\ kPa}$
R^2 (-)	0.788	0.802
ME ($cm^3\ cm^{-3}$)	-0.001	0.001
RMSE ($cm^3\ cm^{-3}$)	0.040	0.033

Table 4

Accuracy of published pedotransfer functions in the estimation of water retention values at -33 and -1500 kPa included in the database.

PTFs	Predictors	RMSE (cm^3 cm^{-3})	
		$\theta_{-33\ kPa}$	$\theta_{-1500\ kPa}$
1. Class-PTFs			
Ramos et al. (2013a)	FAO texture classes	0.055	0.048
	FAO texture classes + depth	0.054	0.047
	FAO texture classes + ρ_b	0.049	0.047
	FAO texture classes + depth + ρ_b	0.047	0.046
	ISSS texture classes	0.049	0.039
	ISSS texture classes + depth	0.047	0.038
	ISSS texture classes + ρ_b	0.042	0.037
Wösten et al. (1999)	FAO texture classes + depth	0.063	0.051
2. Continuous PTFs			
2.1. Point PTFs			
Ramos et al. (2013b)	$Si_{20\ \mu m}$, C, ρ_b, Z	0.040	0.036
2.2. Parametric PTFs			
Gonçalves et al. (1997)	CS, FS, $Si_{20\ \mu m}$, C, ρ_b, Z, OM, pH	0.046	0.053
Wösten et al. (1999)	$Si_{50\ \mu m}$, C, ρ_b, OM, depth	0.049	0.045
Ramos et al. (2013b)	CS, FS, $Si_{20\ \mu m}$, C, ρ_b, Z	0.084	0.051

CS, coarse sand; FS, fine sand; $Si_{20\ \mu m}$, silt fraction at 20 µm; $Si_{50\ \mu m}$, silt fraction at 50 µm; C, clay; ρ_b, bulk density; Z, mean depth; OM, organic matter; depth, qualitative variable having the values 1 (topsoils) and 0 (subsoils).

List of Figures

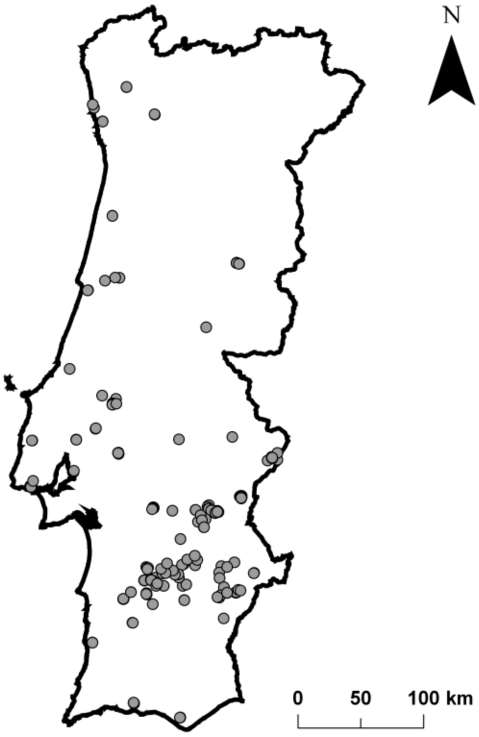

Fig 1. Location of the soil profiles.

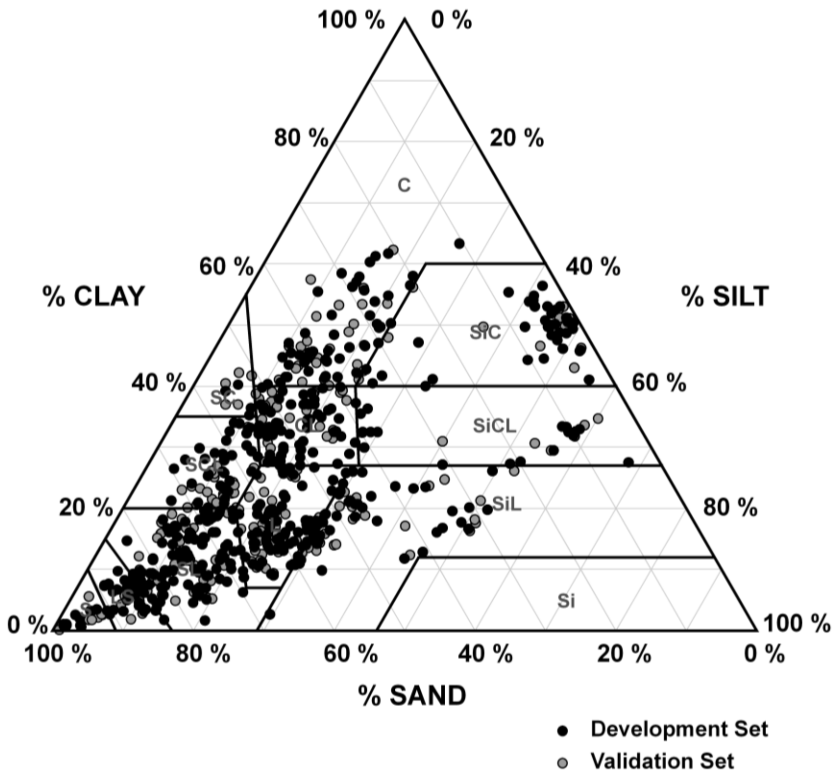

Fig. 2. Textural distribution of the datasets used in the development and validation of the ternary diagrams.

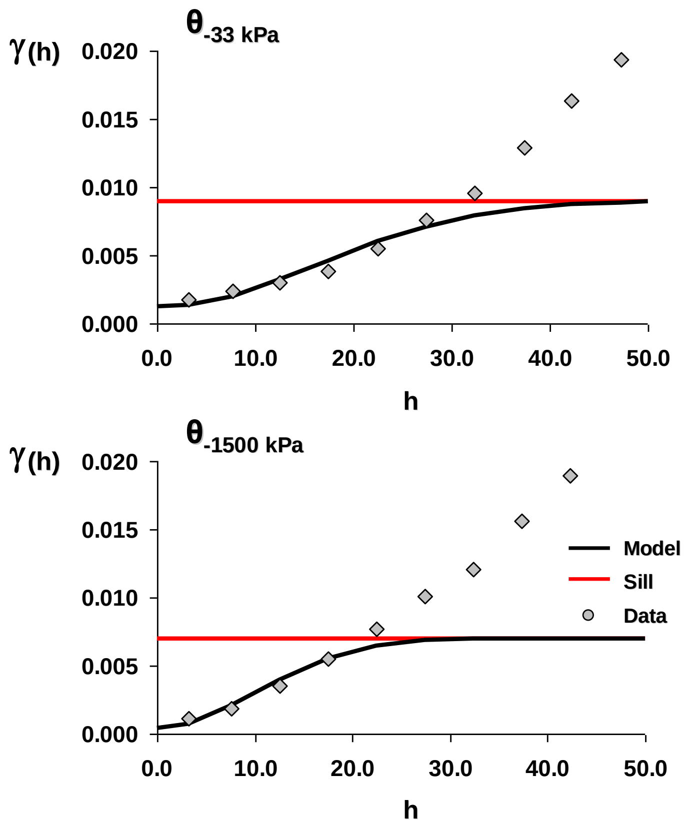

Fig. 3. Experimental semivariogram of $\theta_{-33\ \mathrm{kPa}}$ (top) and $\theta_{-1500\ \mathrm{kPa}}$ (bottom) with the Gaussian model fitted.

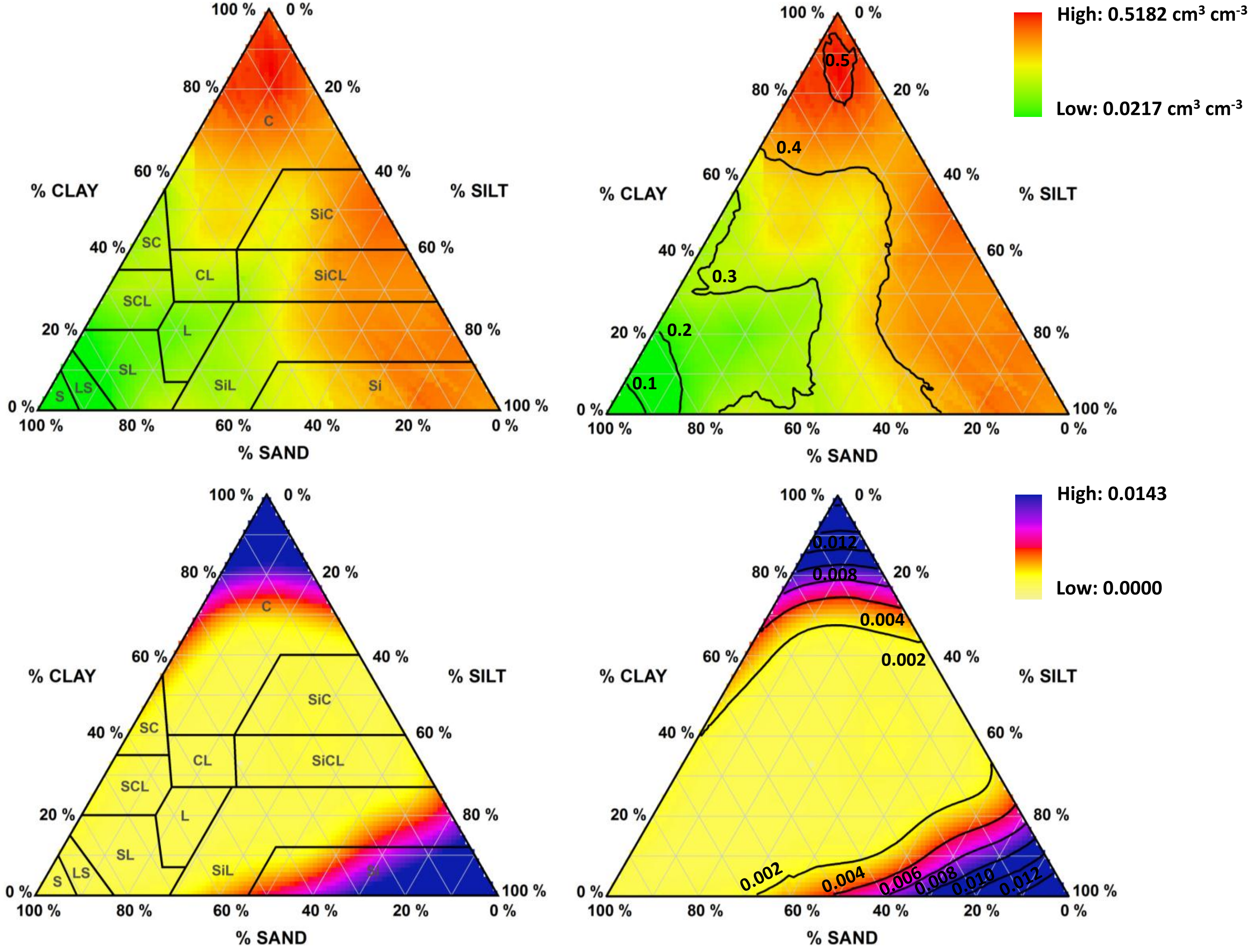

Fig. 4. Ternary diagrams soil water content values at -33 kPa matric potential estimated with ordinary kriging (top) and estimation variance (bottom) of those estimates (figures on the left show the ISSS texture classes; figures on the right show the contour plots of the estimates).

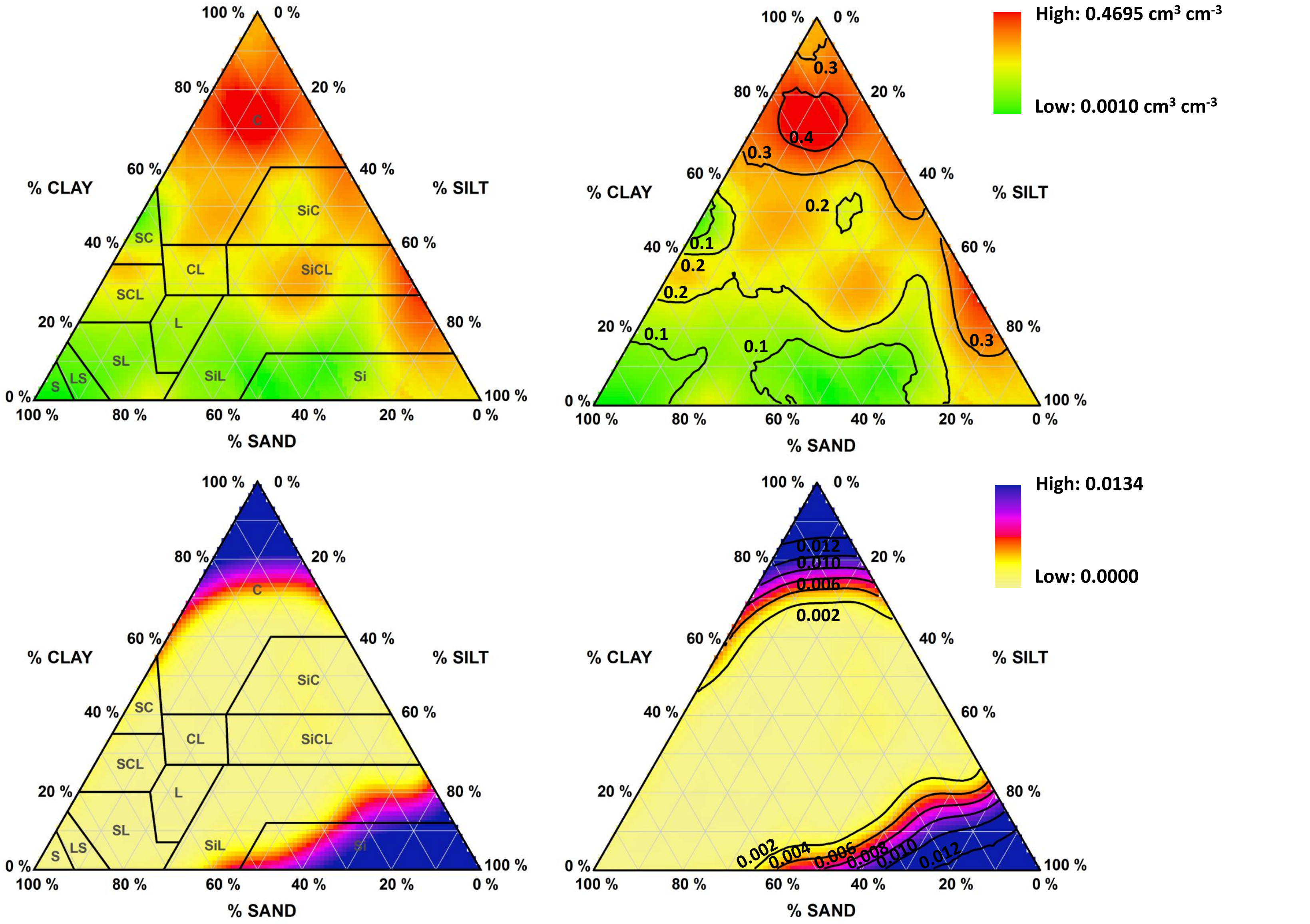

Fig. 5. Ternary diagrams soil water content values at -1500 kPa matric potential estimated with ordinary kriging (top) and estimation variance (bottom) of those estimates (figures on the left show the ISSS texture classes; figures on the right show the contour plots of the estimates).

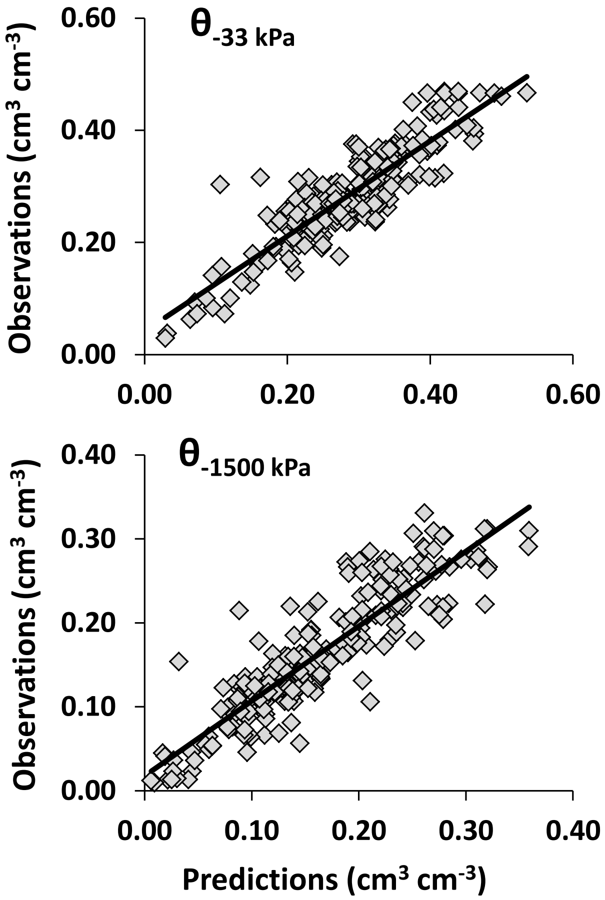

Fig. 6. Scatter plot of prediction of soil water content at -33 and -1500 kPa matric potentials with ordinary kriging versus measured values included in the validation dataset.

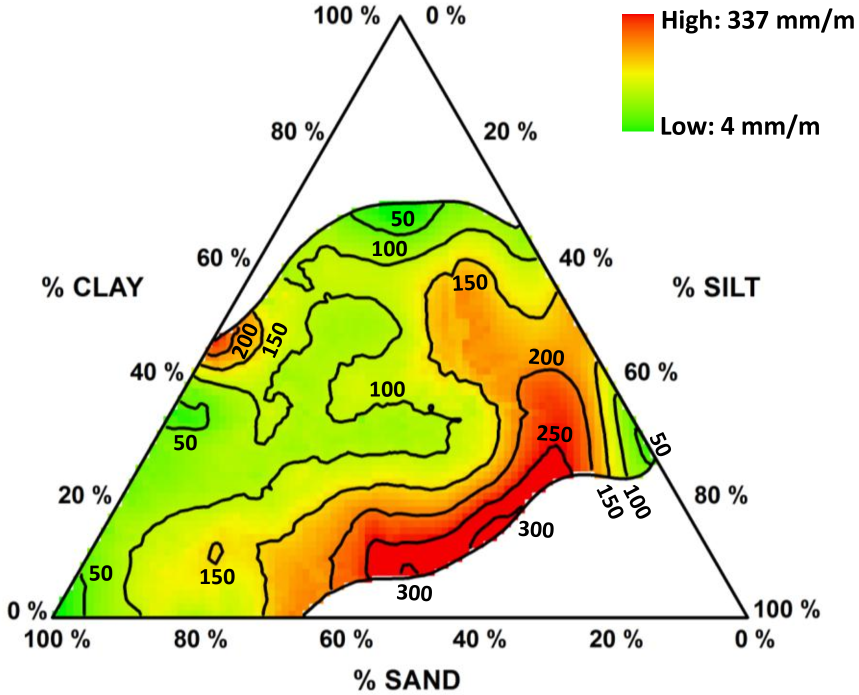

Fig. 7. Ternary diagram with estimates of the available water capacity (AWC).

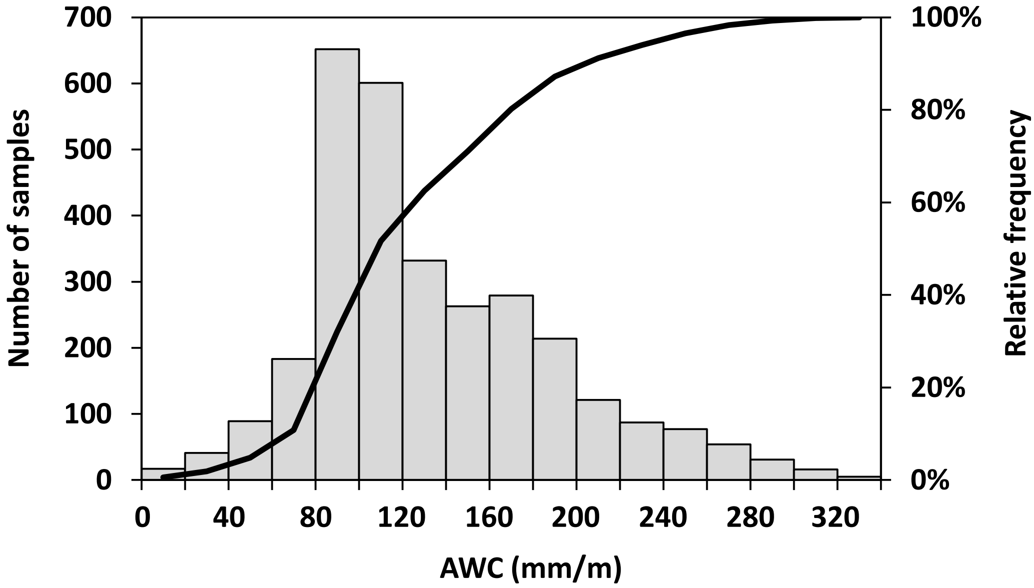

Fig. 8. Histogram with estimates of the available water capacity (AWC).